INTERNATIONAL JOURNAL FOR NUMERICAL METHODS IN FLUIDS, VOL. 17, 115–144 (1993)

NUMERICAL SOLUTIONS OF EULER EQUATIONS BY USING A NEW FLUX VECTOR SPLITTING SCHEME

G-C. ZHA AND E. BILGEN

École Polytechnique, University of Montreal, P.O. Box 6079, St. A Montreal, P.Q., H3C 3A7, Canada

SUMMARY

A new flux vector splitting scheme has been suggested in this paper. This scheme uses the velocity component normal to the volume interface as the characteristic speed and yields the vanishing individual mass flux at the stagnation. The numerical dissipation for the mass and momentum equations also vanishes with the Mach number approaching zero. One of the diffusive terms of the energy equation does not vanish. But the low numerical diffusion for viscous flows may be ensured by using higher-order differencing. The scheme is very simple and easy to be implemented. The scheme has been applied to solve the one dimensional (1D) and multidimensional Euler equations. The solutions are monotone and the normal shock wave profiles are crisp. For a 1D shock tube problem with the shock and the contact discontinuities, the present scheme and Roe scheme give very similar results, which are the best compared with those from Van Leer scheme and Liou–Steffen's advection upstream splitting method (AUSM) scheme. For the multidimensional transonic flows, the sharp monotone normal shock wave profiles with mostly one transition zone are obtained. The results are compared with those from Van Leer scheme, AUSM and also with the experiment.

KEY WORDS Flux vector splitting Euler equations

INTRODUCTION

Since the beginning of 1980s, upwind schemes have become very popular for the sound theoretical basis of characteristic theory for hyperbolic systems and thus for their capability of capturing discontinuities. After the pioneer work of Steger and Warming,[1] Flux Vector Splitting (FVS) scheme first drew the attention of the researchers developing the computer codes using CFD. Roe's flux difference splitting scheme was used frequently since it can take care of both the steady shock and the contact discontinuity. With the appearance of Van Leer's FVS, the application of flux vector splitting scheme with the implicit relaxation algorithms became very attractive for their efficiency, simplicity and ability to capture the sharp shock waves.[2–5] Van Leer's scheme showed better behaviour than the Steger–Warming scheme for its smooth transition of the individual split-flux contributions across eigenvalue sign changes, such as at sonic and stagnation points.[6] Very good representations of the inviscid transonic flows can be obtained by using Van Leer's scheme to solve the Euler equations. Unfortunately, the simplicity of the available flux vector splitting schemes comes at a price of reduced accuracy for the viscous flows due to the large numerical dissipation.[7] The reason is that the individual split mass flux does not vanish with the Mach number reaching zero. The High-Order Polynomial Expansions (HOPE) scheme of Liou and Steffen[8] and the low-diffusion FVS of Van Leer[9] aimed at building up the pure FVS schemes with vanishing mass diffusion. They did achieve the required split mass flux. But the instability and non-monotonicity of the schemes are not acceptable for practical calculations. Efforts have

0271–2091/93/140115–30$20.00

Received September 1992
Revised March 1993

also been attempted to improve the original Van Leer scheme by using some techniques borrowed from flux-difference splitting. First suggested by Hänel and then extended by Van Leer,[9,10] the 'Van Leer–Hänel' 90' scheme using the net mass flux and the one-side velocity and the total enthalpy for the transverse momentum and energy equations obtained accurate temperature profile for the supersonic conical viscous flow. However, a pressure glitch is accompanied with that scheme.[9] A successful and promising scheme was suggested by Liou and Steffen (L/S) for their Advection Upstream Splitting Method (AUSM).[11] They introduced an advective Mach number by combining the split-Mach number contributions from original Van Leer mass splitting. The AUSM scheme is remarkably simple and yields vanishing numerical diffusivity at the stagnation. In a variety of 2D Euler and Navier–Stokes calculations presented in Reference 11, the scheme was as accurate and convergency as Roe's splitting, which was considered as the most accurate by then. AUSM scheme does not need the matrix operation required by Roe scheme and only possesses $O(n)$ operations per grid point instead of $O(n^2)$ for Roe's scheme, where n is the number of the equations. Furthermore, AUSM scheme performed very well for a 2D supersonic flow over a circular blunt body for which Roe scheme gave anomalous solutions. It may be because the original Roe's scheme does not satisfy the entropy law and may admit the non-physical solutions such as the expansion shock waves.[12]

The flux vector splitting scheme suggested in this paper is aimed at obtaining the vanishing individual split mass flux with the Mach number reaching zero and keeping the advantages of the FVS, such as being able to capture the crisp shock profile, the simplicity and the efficiency. The interface flux is divided into two parts according to the eigenvalues, the convective vector and pressure vector. The elements of the vectors are even simpler than AUSM scheme. The eigenvalues of the convective terms, the velocity component normal to the volume interface, are used as the characteristic speeds to attain the goal. The form of the formulations is natural and therefore the simplest. It works soundly to capture the crisp monotone shock wave. Moreover, the present scheme leads to the vanishing numerical dissipation at the stagnation for the mass and momentum equations. Even though one of the diffusive terms of the energy equation does not vanish, the theoretical analysis indicates that small diffusion may be ensured by using higher-order differencing.

THE PRESENT FLUX VECTOR SPLITTING SCHEME

First, we would like to take the 1D Euler equations as the example to explain how the scheme is constructed. The 1D equations are simple and have the similar nature to that of the multidimensions. The 1D Euler equations expressed in Cartesian co-ordinates and conservation form are

$$U_t+F_x=0, \tag{1}$$

where the vectors U and F are given by

$$U=\begin{bmatrix}\rho\\ \rho u\\ e\end{bmatrix}, \qquad F=\begin{bmatrix}\rho u\\ p+\rho u^2\\ (e+p)u\end{bmatrix}, \tag{2}$$

where t is the time, x the distance, ρ the density, u the velocity, p the pressure and e is the specific total energy. The system is closed by an equation of state $p=(\rho, i)$, where i is the specific internal energy ($i=e-1/2\,u^2$). For an ideal gas whose ratio of specific heats is γ, we have

$$p=(\gamma-1)\rho i. \tag{3}$$

Let

$$A=\frac{\partial F}{\partial U}, \tag{4}$$

where A is the 3×3 Jacobian matrix. It is already well known that the matrix has three real eigenvalues, u, $u+a$, $u-a$, where a is the sound speed introduced as

$$a^2=\frac{\partial p}{\partial \rho}=\frac{\gamma p}{\rho}. \tag{5}$$

The following equation can be derived by splitting the diagonal eigenvalue matrix to two parts:

$$F=AU=Q\Lambda Q^{-1}U=Q\begin{bmatrix}u&0&0\\0&u&0\\0&0&u\end{bmatrix}Q^{-1}U+Q\begin{bmatrix}0&0&0\\0&a&0\\0&0&-a\end{bmatrix}Q^{-1}U=C+P, \tag{6}$$

where C and P represent the convective and pressure terms and are expressed as the following vectors:

$$C=u\begin{bmatrix}\rho\\ \rho u\\ e\end{bmatrix},\qquad P=\begin{bmatrix}0\\ p\\ pu\end{bmatrix}. \tag{7}$$

Obviously, the eigenvalues of the Jacobian of C and P are (u, u, u) and $(0, a, -a)$, respectively. This suggests that the information of the convective terms propagates uniformly in the same direction as the velocity vector u goes, and the information of the pressure terms goes with the convective terms at the speed u and propagates in all directions at the sound speed a. The present scheme is contrived to evaluate the interface flux $F_{i+1/2}$ at locations such as $(i+1/2\,\Delta x)$ according to the information travel directions of vector C and P, respectively.

The following is the details of the present scheme:

$$F_{i+1/2}=F_{\mathrm{L}}^{+}+F_{\mathrm{R}}^{-}. \tag{8}$$

For subsonic flow, $|u|<a$, the pressure terms are determined by

$$P_{i+1/2}=P_{\mathrm{L}}^{+}+P_{\mathrm{R}}^{-},\quad \text{where}\quad P^{\pm}=\frac{1}{2}\begin{bmatrix}0\\ p(1\pm M)\\ p(u\pm a)\end{bmatrix}. \tag{9}$$

The convective terms are

$$\text{if}\quad a>u\geq 0,\quad C_{i+1/2}=C_{\mathrm{L}}^{+}+C_{\mathrm{R}}^{-},\quad \text{where}\quad C_{\mathrm{L}}^{+}=C_{\mathrm{L}},\quad C_{\mathrm{R}}^{-}=0, \tag{10}$$

$$\text{if}\quad -a<u<0,\quad C_{i+1/2}=C_{\mathrm{L}}^{+}+C_{\mathrm{R}}^{-},\quad \text{where}\quad C_{\mathrm{L}}^{+}=0,\quad C_{\mathrm{R}}^{-}=C_{\mathrm{R}}, \tag{11}$$

$$F_{\mathrm{L}}^{+}=C_{\mathrm{L}}^{+}+P_{\mathrm{L}}^{+}, \tag{12}$$

$$F_{\mathrm{R}}^{-}=C_{\mathrm{R}}^{-}+P_{\mathrm{R}}^{-}, \tag{13}$$

Thus equation (8) can be written as the following general and simple form:

$$F_{i+1/2}=\frac{1}{2}(F_{\mathrm{L}}+F_{\mathrm{R}})-\frac{1}{2}\left[\left[|u|\begin{bmatrix}\rho\\ \rho u\\ e\end{bmatrix}+\begin{bmatrix}0\\ pM\\ pa\end{bmatrix}\right]_{\mathrm{R}}-\left[\left[|u|\begin{bmatrix}\rho\\ \rho u\\ e\end{bmatrix}+\begin{bmatrix}0\\ pM\\ pa\end{bmatrix}\right]_{\mathrm{L}}\right]. \tag{14}$$

For supersonic flow, it is the same as the standard upwind differencing scheme, i.e.

$$F_{i+1/2}=F_L^+ + F_R^-, \tag{15}$$

$$\text{if} \quad u \geq a, \qquad F^+ = F_L, \quad F^- = 0, \tag{16}$$

$$\text{if} \quad u \leq -a, \quad F_L^+ = 0, \qquad F_R^- = F_R. \tag{17}$$

It can be proven that the eigenvalues of P^+ and P^- are non-negative and non-positive for the flows with $\gamma \geq 1$. The pressure splitting for momentum equation is taken from L/S AUSM scheme. The pressure power term in the energy equation is split using a similar idea. The whole pressure splitting is based on the acoustic propagation speeds $(u \pm a)$ or their weights $(M \pm 1)$ for average. This may represent the pressure propagation characteristics.

It is clear that the split flux is continuous everywhere. It leads to standard upwind scheme in the supersonic region. The mass flux is the same as the natural one and therefore also continuously differentiable everywhere. As shown in Figure 1, the individual mass flux vanishes with the Mach number approaching zero, while those of Van Leer's FVS and Steger–Warming's FVS do not vanish. However, the individual split flux for pressure term is not continuously differentiable across the sonic point. When first-order differencing is used this will cause a glitch at the sonic point similar to that of Steger–Warming scheme. Fortunately, this glitch can be removed automatically by using higher-order differencing. Liou and Steffen[11] reported that this pressure splitting could get smoother transition across the sonic point than the continuously differentiable one with the higher-order polynomial. This may be true only when higher-order differencing is used. The advantage of this pressure splitting is that it can obtain the monotone shock profile even when the second-order differencing is used. At the stagnation point, unlike the Steger–Warming scheme, the present scheme is continuously differentiable.

NUMERICAL DIFFUSION OF THE SCHEME

From equation (14), it is seen that the present flux vector splitting scheme can be exactly written as a central differencing plus the diffusive terms. For supersonic flow, the diffusion is the same as the standard upwind scheme. The focus here is concentrated in the subsonic region. Let

$$D=|u|\begin{bmatrix}\rho\\ \rho u\\ e\end{bmatrix}+\begin{bmatrix}0\\ pM\\ pa\end{bmatrix} \tag{18}$$

the diffusive vector, namely D_{dif}, can be expressed as

$$D_{dif}=\tfrac{1}{2}(D_R - D_L). \tag{19}$$

Equation (14) can then be rewritten as

$$F_{i+1/2}=\tfrac{1}{2}[F_L+F_R]-D_{dif}. \tag{20}$$

For the extrapolation schemes with different-order accuracy, the accuracy order of D_{dif} is also different. D_{dif} is equivalent to adding the following derivatives into Euler equations.

For first-order fully upwind extrapolation:

$$D_{dif}=\frac{1}{2}\frac{\partial^2 D}{\partial x^2}\Delta x. \tag{21}$$

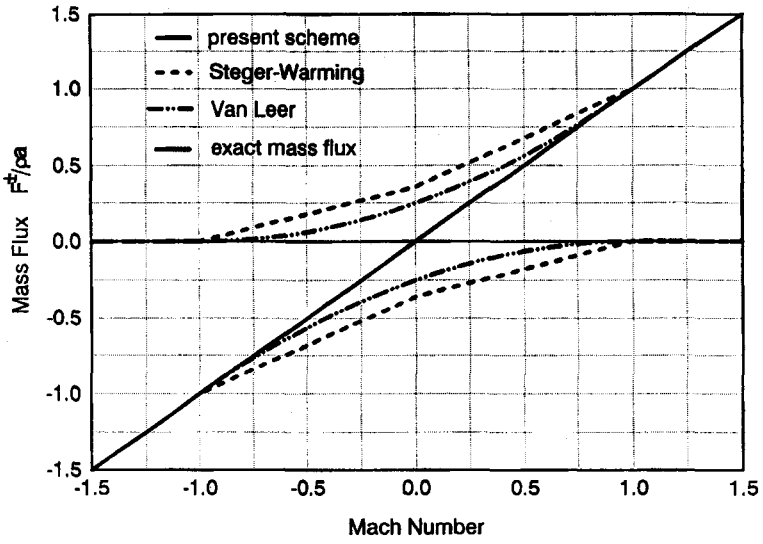

Figure 1. Mass flux of the flux vector splitting schemes

For second-order fully upwind extrapolation:

$$D_{\text{dif}} = -\frac{1}{4}\frac{\partial^4 D}{\partial x^4}\Delta x^3. \tag{22}$$

For third-order upwind-biased extrapolation:

$$D_{\text{dif}} = -\frac{1}{12}\frac{\partial^4 D}{\partial x^4}\Delta x^3. \tag{23}$$

From equation (18), it can be seen that almost all the diffusive terms vanish at the stagnation except only one term, pa, in the energy equation. The vanishing terms may ensure that their diffusion is small. As equations (22) and (23) show, if a higher-order differencing is used, the low diffusion may be furthermore ensured by the higher-order derivatives and the higher power of the grid spacing. The diffusion generated by pa,

$$-\frac{1}{4}\frac{\partial^4 pa}{\partial x^4}\Delta x^3 \quad \text{or} \quad -\frac{1}{12}\frac{\partial^4 pa}{\partial x^4}\Delta x^3,$$

may also be expected to remain small.

In many cases, the gradient of pa near the solid wall may be small. Particularly, for some practical cases, when the sound speed is only considered as the function of temperature as the ideal gas, if the wall is adiabatic and the pressure gradient normal to the wall is zero or small enough to be treated as zero, the diffusion of pa will disappear by cancellation, and therefore the total diffusion will disappear on the wall no matter which order of differencing is used.

Further computational experiments will be made in a later study to investigate the effect of the numerical diffusion of the present scheme for the viscous flow calculations.

For the ability of the present scheme to capture shock waves, it is not proven here by analysis how sharp the shock wave profile will be. But the computational experiments presented later show that the normal shock captured is as crisp as that obtained by using the Roe scheme and is at most two transition zones.

One obvious advantage of the present scheme is its simplicity. Similar to Van Leer and L/S AUSM schemes, it does not need the matrix operations required by Roe scheme. The formulations are polynomial in M (Mach number) and of degree one, which is the lowest possible degree. The implementation of this scheme is even easier than AUSM scheme. Although AUSM scheme is already very simple, its interface Mach number containing both left- and right-hand-side variables is not so convenient to get the Jacobian matrix when implicit discretization is to be implemented. The interface flux of the present scheme is composed of the vectors with the pure left-hand-side variables and the pure right-hand-side variables like Van Leer scheme. It is straightforward to construct the implicit operator.

THE ADVECTION UPSTREAM SPLITTING METHOD (AUSM)

As mentioned in the introduction, the AUSM scheme suggested by Liou and Steffen[11] is a simple scheme with good accuracy. Hence, the results of the present scheme are compared to the results calculated by using the AUSM scheme. As the AUSM scheme is relatively new, a brief description of it in 1D form is given.

The flux F given in equation (2) can be written as

$$F = u\begin{bmatrix}\rho\\ \rho u\\ \rho H\end{bmatrix} + \begin{bmatrix}0\\ p\\ 0\end{bmatrix} = M\begin{bmatrix}\rho a\\ \rho u a\\ \rho H a\end{bmatrix} + \begin{bmatrix}0\\ p\\ 0\end{bmatrix}, \tag{24}$$

where H is the enthalpy.

For subsonic flow, the flux at the interface $L<1/2<R$ is given as follows: Let

$$E = \begin{bmatrix}\rho a\\ \rho a u\\ \rho a H\end{bmatrix}, \tag{25}$$

$$F_{1/2} = M_{1/2}\frac{1}{2}[E_L + E_R] - \frac{1}{2}|M_{1/2}|\,\Delta_{1/2}E + \begin{bmatrix}0\\ P_L^+ + P_R^-\\ 0\end{bmatrix}, \tag{26}$$

where

$$M_{1/2} = M_L^+ + M_R^-. \tag{27}$$

The Van Leer's splitting is used to evaluate $M^\pm$, i.e. $M^\pm = \pm\frac{1}{4}(M\pm 1)^2$, where $\Delta_{1/2}E$ means

$$\Delta_{1/2}E = E_R - E_L. \tag{28}$$

There are two choices for the pressure splitting. The first one is the third-order polynomial of M and is expressed as

$$P^\pm = \frac{P}{4}(M\pm 1)^2(2\mp M). \tag{29}$$

The second one is the simplest possible form of the lowest order

$$P^\pm = \frac{P}{2}(1\pm M). \tag{30}$$

Choice 2 can give a monotone shock profile and choice 1 may yield oscillations near the shock. The interface flux for supersonic flow is set as usual by taking either the left or right state depending on the sign of the Mach number.

EXTENSION AND APPLICATION OF THE PRESENT SCHEME TO MULTIDIMENSIONAL EULER EQUATIONS

Governing equations

The non-dimensional form of the 3D equations in conservation law form and in Cartesian co-ordinates is given as

$$\frac{\partial U}{\partial t}+\frac{\partial F}{\partial x}+\frac{\partial G}{\partial y}+\frac{\partial H}{\partial z}=0, \tag{31}$$

where

$$U=\begin{bmatrix}\rho\\ \rho u\\ \rho v\\ \rho w\\ e\end{bmatrix},\quad F=\begin{bmatrix}\rho u\\ p+\rho u^2\\ \rho uv\\ \rho uw\\ (e+p)u\end{bmatrix},\quad G=\begin{bmatrix}\rho v\\ \rho uv\\ p+\rho v^2\\ \rho vw\\ (e+p)v\end{bmatrix},\quad H=\begin{bmatrix}\rho w\\ \rho uw\\ \rho vw\\ p+\rho w^2\\ (e+p)w\end{bmatrix}. \tag{32}$$

The velocities are u, v, w and e is the total energy per unit volume. The pressure p is determined by the ideal gas law

$$p=(\gamma-1)[e-\gamma(u^2+v^2+w^2)/2], \tag{33}$$

where γ is the ratio of specific heats, taken as $\gamma=1{\cdot}4$.

To discretize the equations using finite volume method, the equations should be written in the integral form. Let

$$R=F\mathbf{i}_x+G\mathbf{i}_y+H\mathbf{i}_z. \tag{34}$$

Using the Gauss theorem, the integral form of equation (31) is

$$\int_Q U\,\mathrm{d}Q+\int_S R\mathbf{n}\,\mathrm{d}S=0, \tag{35}$$

where Q is the volume bounded by the surface S and n is the outward pointing unit vector normal to the surface. $\mathbf{n}$ is expressed as

$$n=n_x\mathbf{i}_x+n_y\mathbf{i}_y+n_z\mathbf{i}_z. \tag{36}$$

The equations are discretized in the physical domain on the arbitrary body-fitted grid.

Three-dimensional form of the present upwind scheme

The flux crossing an interface of two adjacent cells is the normal component of vector R given in equation (34). Let Z be the normal component passing through unit interface. Thus,

$$Z=Rn=Fn_x+Gn_y+Hn_z, \tag{37}$$

$$=U_n\begin{bmatrix}\rho\\ \rho u\\ \rho v\\ \rho w\\ e\end{bmatrix}+\begin{bmatrix}0\\ pn_x\\ pn_y\\ pn_z\\ pU_n\end{bmatrix}=C+P, \tag{38}$$

where U_n is the normal component of the velocity expressed as

$$U_n=un_x+vn_y+wn_z, \tag{39}$$

Z will be evaluated by using the present flux vector splitting scheme. The extension of the scheme from 1D to 3D is straightforward. Similar to the 1D case, the eigenvalues of the Jacobian matrix of the convective vector are U_n. The eigenvalues for the pressure term matrix are still $\pm a$. C and P in equation (38) stand again for the convective and pressure terms. Using the eigenvalues of the convective term Jacobian matrix as the characteristic speed, the 3D form of this flux vector splitting scheme can be expressed as

$$Z_{1/2}=Z_{\mathrm{L}}^{+}+Z_{\mathrm{R}}^{-}. \tag{40}$$

For subsonic flow, $|U_n|<a$, the pressure terms are

$$P_{i+1/2}=P_{\mathrm{L}}^{+}+P_{\mathrm{R}}^{-}=\frac{1}{2}\begin{bmatrix}0\\ p(1+M_n)n_x\\ p(1+M_n)n_y\\ p(1+M_n)n_z\\ p(U_n+a)\end{bmatrix}_{\mathrm{L}}+\frac{1}{2}\begin{bmatrix}0\\ p(1-M_n)n_x\\ p(1-M_n)n_y\\ p(1-M_n)n_z\\ p(U_n-a)\end{bmatrix}_{\mathrm{R}} \tag{41}$$

The convective terms are

$$\text{if}\quad a>U_n\geq 0,\quad C_{i+1/2}=C_{\mathrm{L}}^{+}+C_{\mathrm{R}}^{-},\quad \text{where}\quad C_{\mathrm{L}}^{+}=C_{\mathrm{L}},\quad C_{\mathrm{R}}^{-}=0, \tag{42}$$

$$\text{if}\quad -a>U_n<0,\quad C_{i+1/2}=C_{\mathrm{L}}^{+}+C_{\mathrm{R}}^{-},\quad \text{where}\quad C_{\mathrm{L}}^{+}=0,\quad C_{\mathrm{R}}^{-}=C_{\mathrm{R}}, \tag{43}$$

$$F_{\mathrm{L}}^{+}=C_{\mathrm{L}}^{+}+P_{\mathrm{L}}^{+}, \tag{44}$$

$$F_{\mathrm{R}}^{-}=C_{\mathrm{R}}^{-}+P_{\mathrm{R}}^{-}. \tag{45}$$

Let

$$D=|U_n|\begin{bmatrix}\rho\\ \rho u\\ \rho v\\ \rho w\\ e\end{bmatrix}+\begin{bmatrix}0\\ pM_nn_x\\ pM_nn_y\\ pM_nn_z\\ pa\end{bmatrix}$$

The general form of the present scheme in 3D is given as

$$Z_{1/2}=\tfrac{1}{2}(Z_{\mathrm{L}}+Z_{\mathrm{R}})-\tfrac{1}{2}(D_{\mathrm{R}}-D_{\mathrm{L}}). \tag{46}$$

For supersonic flow

$$\text{if}\quad U_n\geq a,\qquad F_{\mathrm{L}}^{+}=F_{\mathrm{L}},\quad F_{\mathrm{R}}^{-}=0, \tag{47}$$

$$\text{if}\quad U_n\leq -a,\quad F_{\mathrm{L}}^{+}=0,\qquad F_{\mathrm{R}}^{-}=F_{\mathrm{R}}. \tag{48}$$

The Mach number M_n is based on the normal component of the velocity, $M_n=U_n/a$. The diffusion terms corresponding to equations (21)–(23) are changed now to the following forms.

For first-order fully upwind extrapolation:

$$D_{\mathrm{dif}}=\frac{1}{2}\frac{\partial^2 D}{\partial n^2}\Delta n. \tag{49}$$

For second-order fully upwind extrapolation:

$$D_{\mathrm{dif}}=-\frac{1}{4}\frac{\partial^4 D}{\partial n^4}\Delta n^3. \tag{50}$$

For third-order upwind-biased extrapolation:

$$D_{\text{dif}} = -\frac{1}{12}\frac{\partial^4 D}{\partial n^4}\Delta n^3. \tag{51}$$

BOUNDARY CONDITIONS

The conditions for slip and adiabatic wall are used on the solid surfaces. The flux on the wall is

$$Z_W = [0 \quad p_w n_w \quad p_w n_y \quad p_w n_z \quad 0]^{\mathrm{T}}. \tag{52}$$

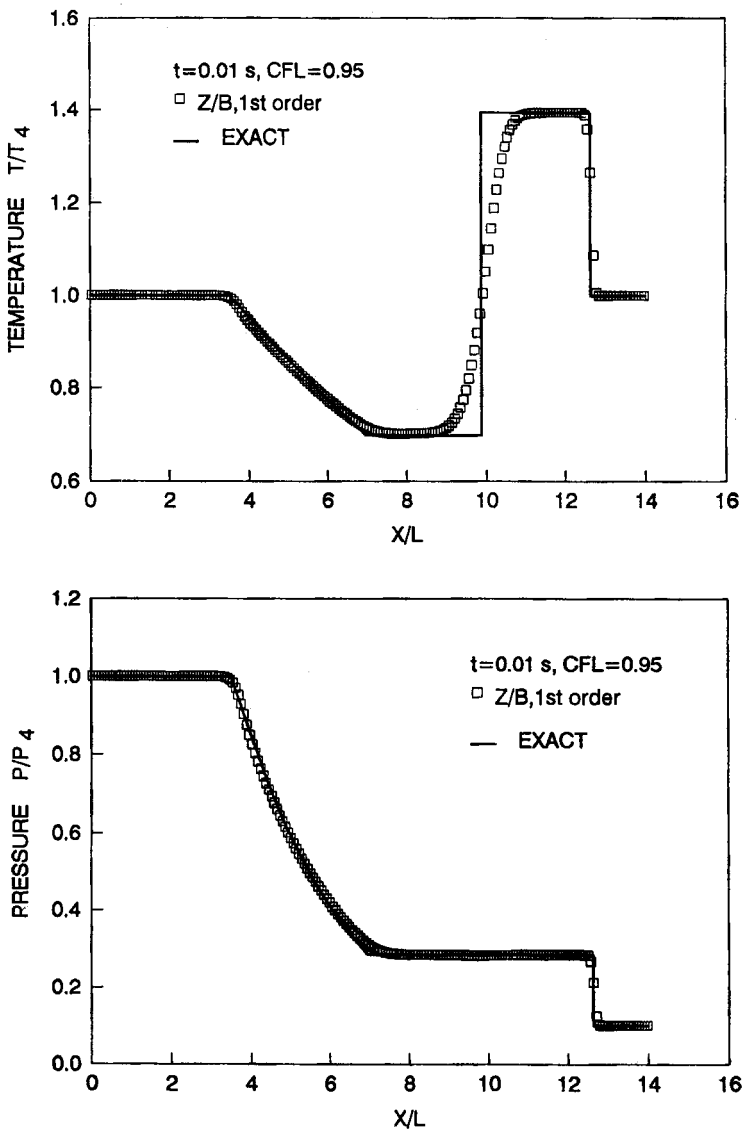

Figure 2. 1D shock tube results calculated by using the present scheme, grid size: 201, temperature and pressure

The pressure is first-order extrapolated from the inner points. On the implicit side,

$$\delta Z_W^{n+1} = \frac{\partial Z_W}{\partial U} \delta U^{n+1}, \tag{53}$$

where $\partial Z_W / \partial U$ is the Jacobian matrix and incorporated into the matrix equations when the implicit algorithms are used. At the inlet and the exit, the number of the variables determined from the inner points is based on the characteristic line theory and the variables are first-order extrapolated.

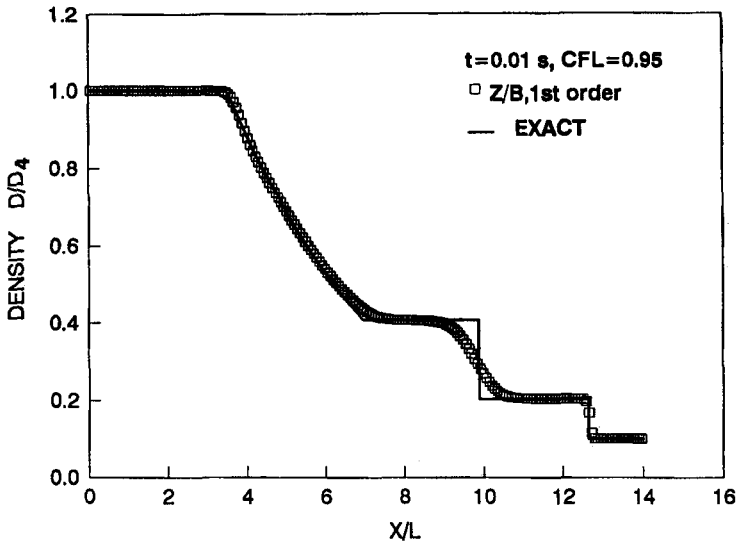

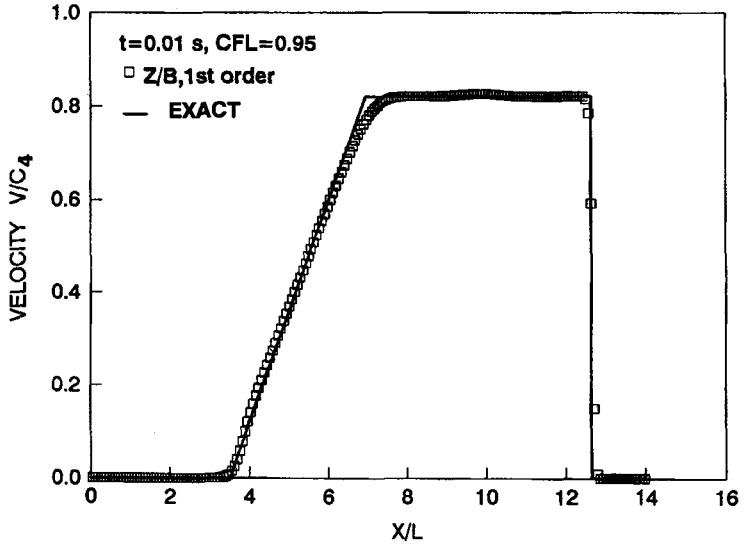

Figure 3. 1D shock tube results calculated by using the present scheme, grid size: 201, density and velocity

RESULTS AND DISCUSSION

To judge the viability of the present scheme, 1D, 2D and 3D Euler equations were solved.

Case 1: Case 1 is a 1D shock tube flow. As a model problem, consider a tube of large extent in which a diaphragm separates a perfect gas at rest with different static pressures but at a uniform temperature. With the rupture of the diaphragm, an expansion propagates into the high-pressure gas, while a shock wave, followed by a contact discontinuity, propagates into the low-pressure

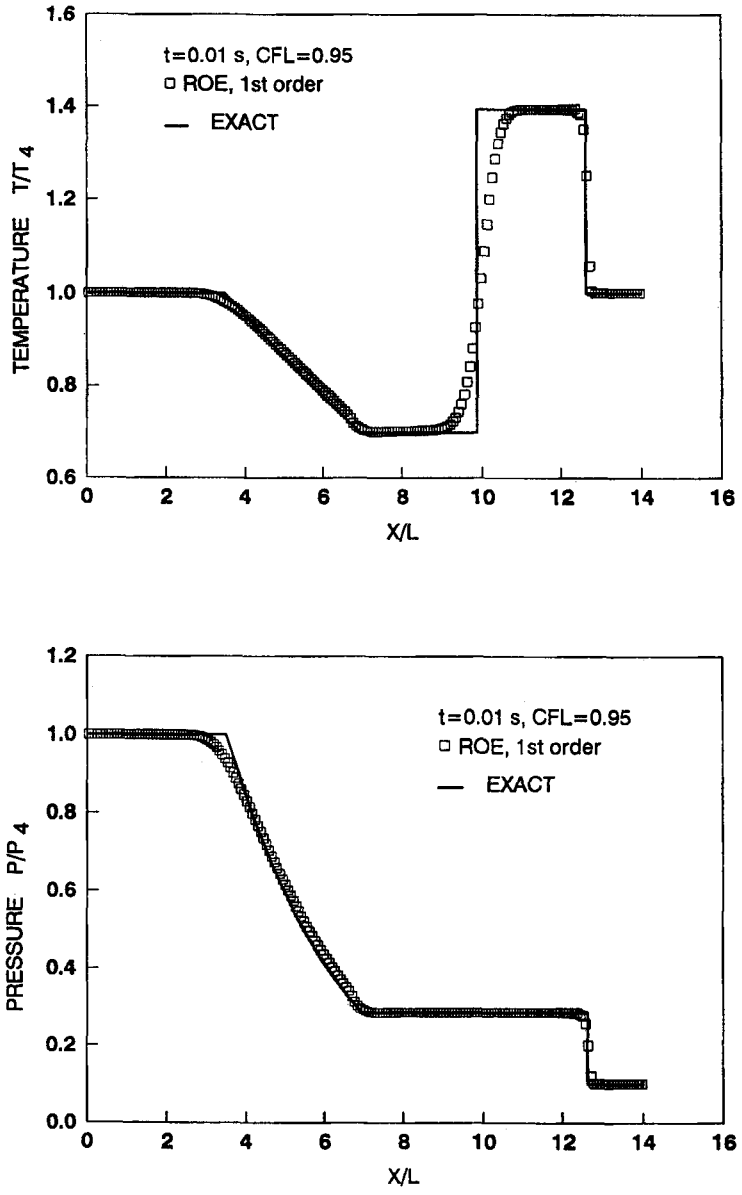

Figure 4. 1D shock tube results calculated by using Roe scheme, grid size: 201, temperature and pressure

gas. Details of this flow are described in standard texts.[16] In the present calculations, the initial pressure ratio across the diaphragm is taken as 10 to 1. The initial location of the diaphragm is taken at $X/L=7{\cdot}0$. To compare the present scheme with the others, Roe's flux difference splitting scheme, Van Leer's flux vector splitting scheme and Liou–Steffen's AUSM scheme were also used to solve the same 1D problem. All the solutions were calculated by using the explicit first-order accuracy differencing. Figures 2 and 3 are the solutions of the present scheme with the CFL number 0·95. The solutions are monotone. A crisp shock profile is seen, while the contact

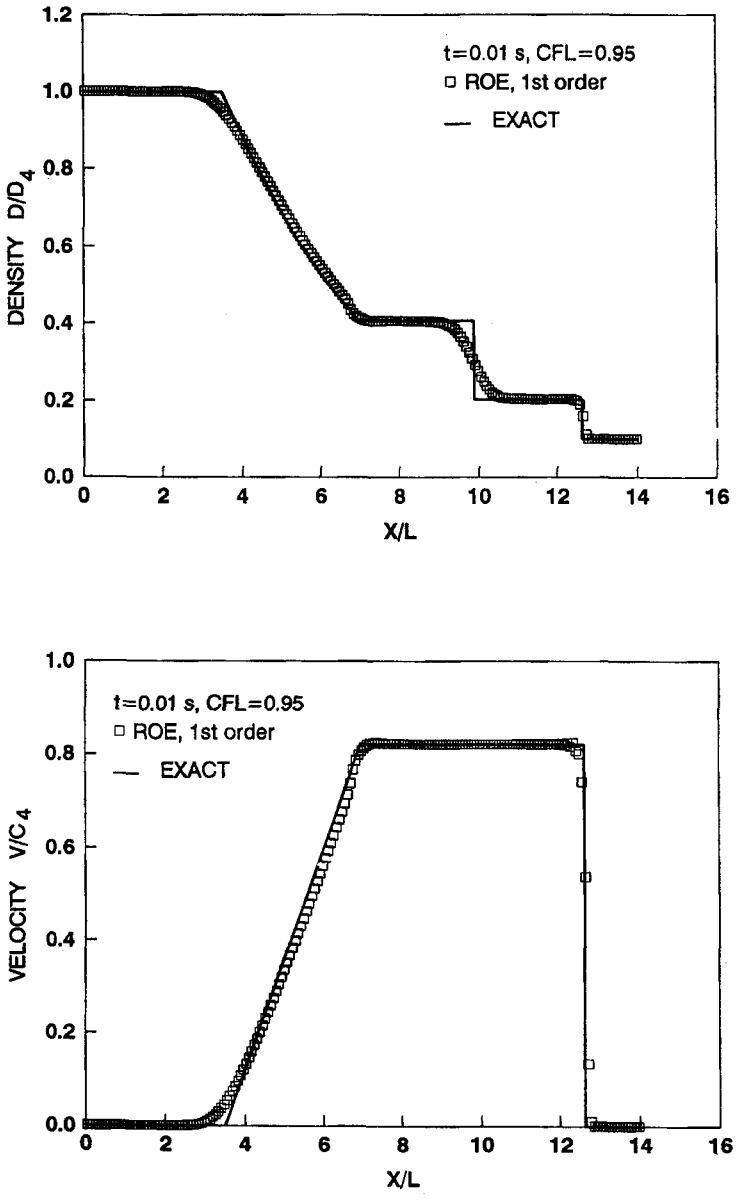

Figure 5. 1D shock tube results calculated by using Roe scheme, grid size: 201, density and velocity

discontinuity is composed of more grid zones. It is seen that the present scheme also gives good agreement with the exact solution for the expansion waves. The solutions of Roe's scheme are shown in Figures 4 and 5. The shock wave and the contact discontinuity profiles show no distinguishable difference between the solution of the present scheme and the Roe scheme. In comparing the results, the front of the expansion waves calculated by the present scheme is sharper than that of Roe's scheme. It is noted however that the results of the both schemes agree well with the exact solution. Figures 6 and 7 show the results of Van Leer scheme when the CFL

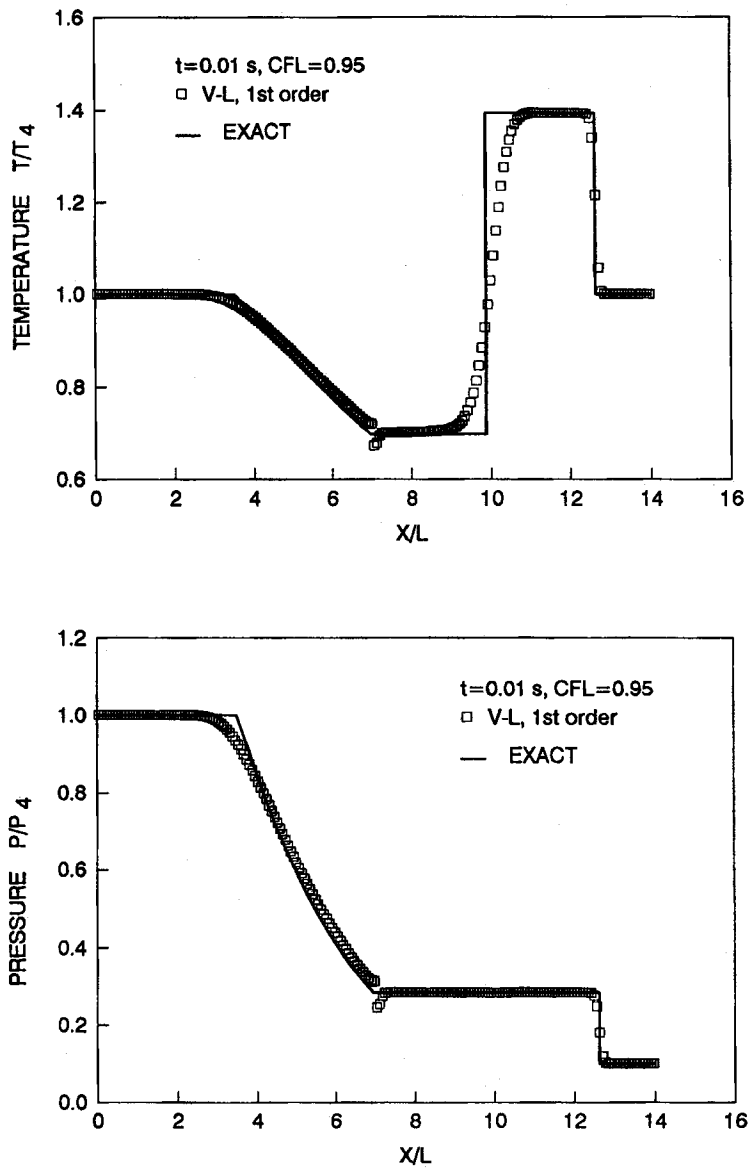

Figure 6. 1D shock tube results calculated by using Van Leer scheme, grid size: 201, temperature and pressure

number is 0·95. The profiles of the shock and the discontinuity are basically the same as those of the present scheme and Roe scheme. But there are large spikes at the tail of the expansion waves for all the parameters. The computational experiments indicated that the spikes became less when the CFL number was decreased. The spikes basically disappeared when the CFL number was down to 0·45 at a loss of sharp shock profiles as can be seen in Figures 8 and 9. Figures 10 and 11 present the results of the AUSM scheme. It was noted that the CFL number for AUSM scheme could not be greater than 0·4 for this 1D shock tube problem; otherwise, the iteration became

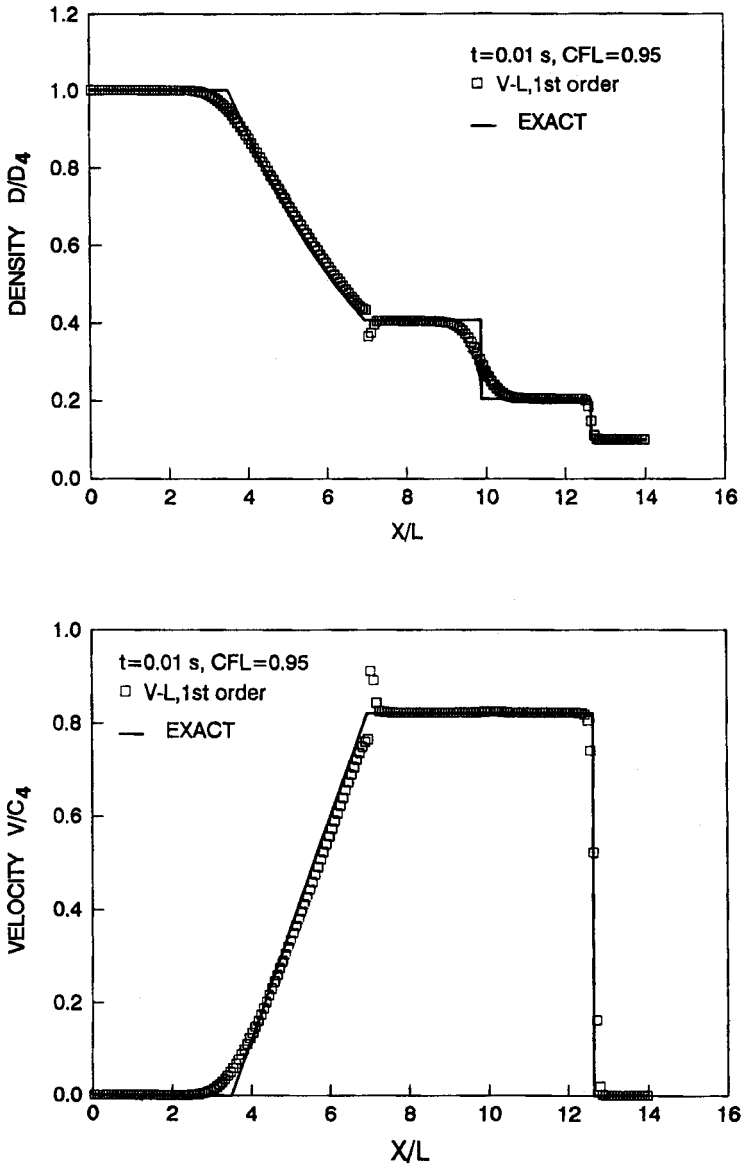

Figure 7. 1D shock tube results calculated by using Van Leer scheme, grid size: 201, density and velocity

unstable. The maximum CFL number used in our calculation for the AUSM scheme was 0·35. Similarly, with Van Leer scheme when the CFL number was 0·45 as shown in Figures 8 and 9, both the shock and the contact discontinuities were somewhat diffused because the CFL number was far from the upper limit of the explicit scheme, CFL = 1. As indicated in Reference 14, this is a common phenomenon for most of the differencing schemes. Among these four schemes tested for this 1D shock tube problem, only the present scheme and the Roe's scheme gave the most satisfactory results.

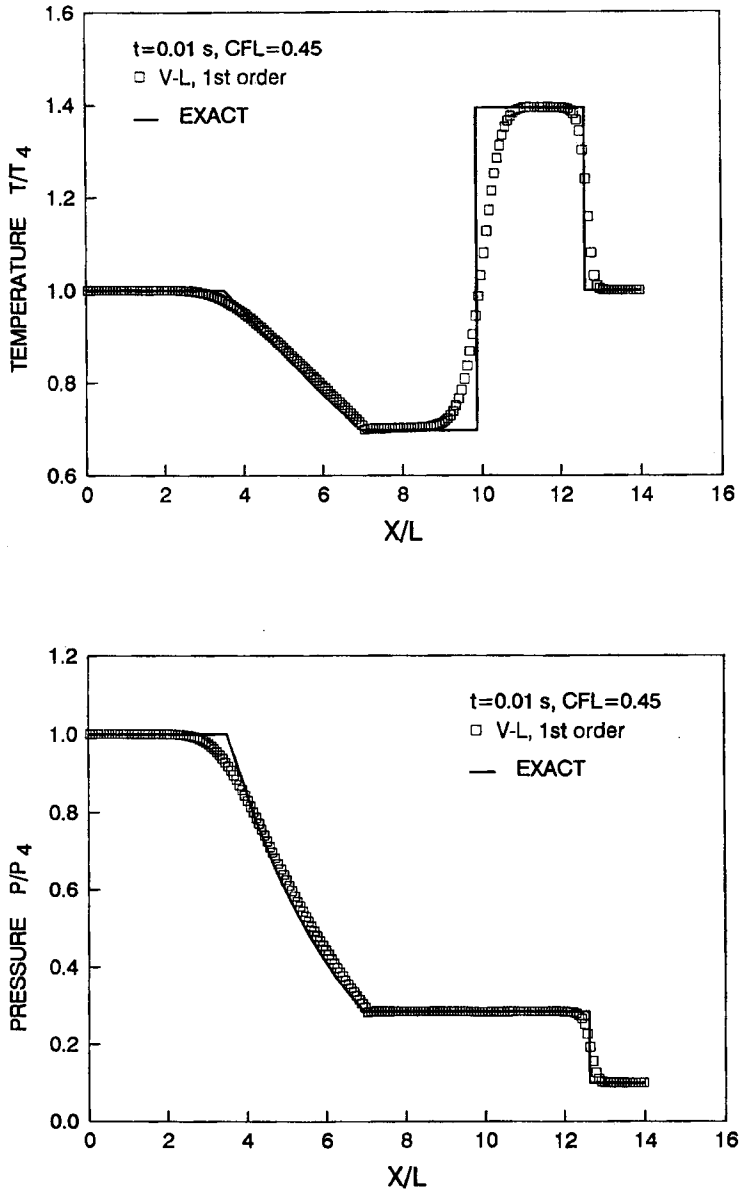

Figure 8. 1D shock tube results calculated by using Van Leer scheme, grid size: 201, temperature and pressure

Case 2: Case 2 is a 2D transonic Inlet-diffuser shown in Figure 12 designed and studied by Bogar *et al.*[18] It is a 3D diffuser that can also be treated as 2D. It contains a normal shock wave in the downstream of its throat. The calculation was implemented first using first-order differencing on the streamwise plane as a 2D case. The explicit two-stage method[15] was used for the present scheme and AUSM scheme and the 2D implicit upwind-relaxation method for the Van Leer scheme.[4] Because the implicit operator with the first-order differencing was used for the Van Leer

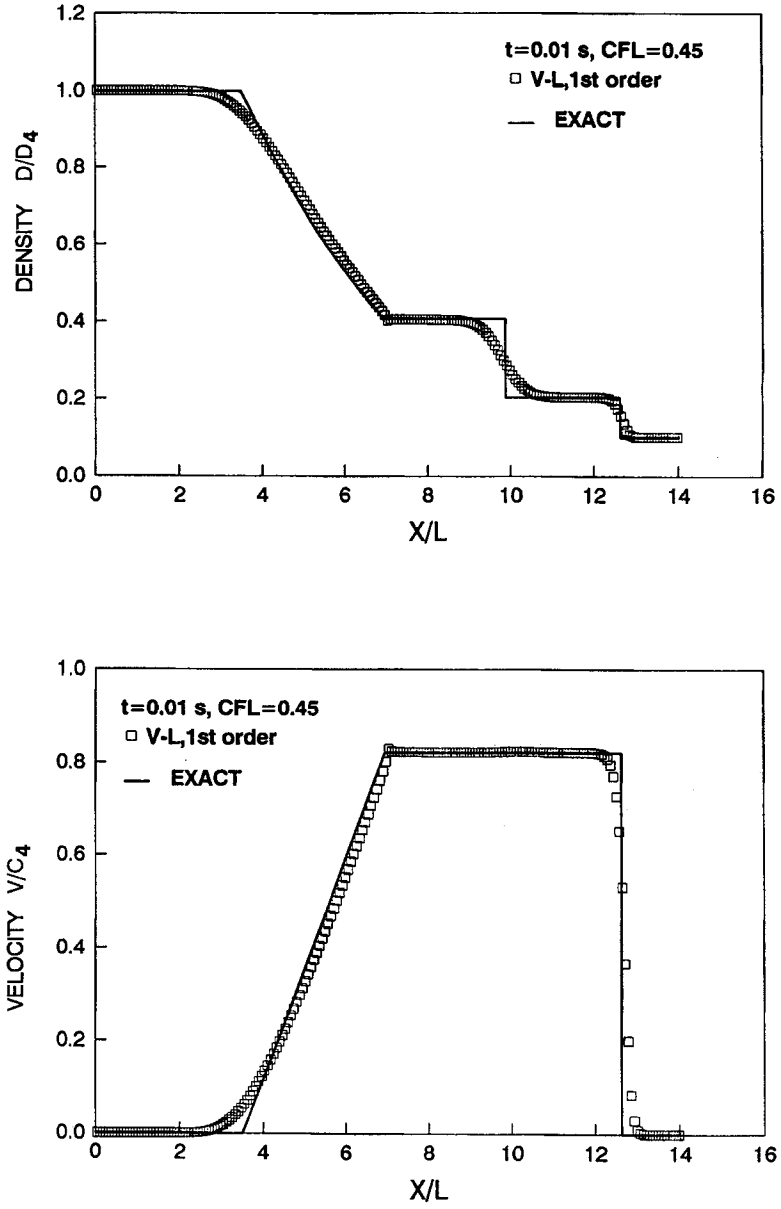

Figure 9. 1D shock tube results calculated by using Van Leer scheme, grid size: 201, density and velocity

scheme, the calculation only converged for the RHS with first- and third-order accuracy differencing. Therefore, the results of Van Leer scheme will be presented only for the first- and third-order differencing. Figure 13 shows the Mach number distributions along the bottom and top walls. It is seen that the shock profiles are very sharp. The Mach number transition from the supersonic peak to the subsonic bottom takes only one grid width for both the present and the AUSM scheme. The Van Leer scheme needs two transition zones. All these three shock profiles

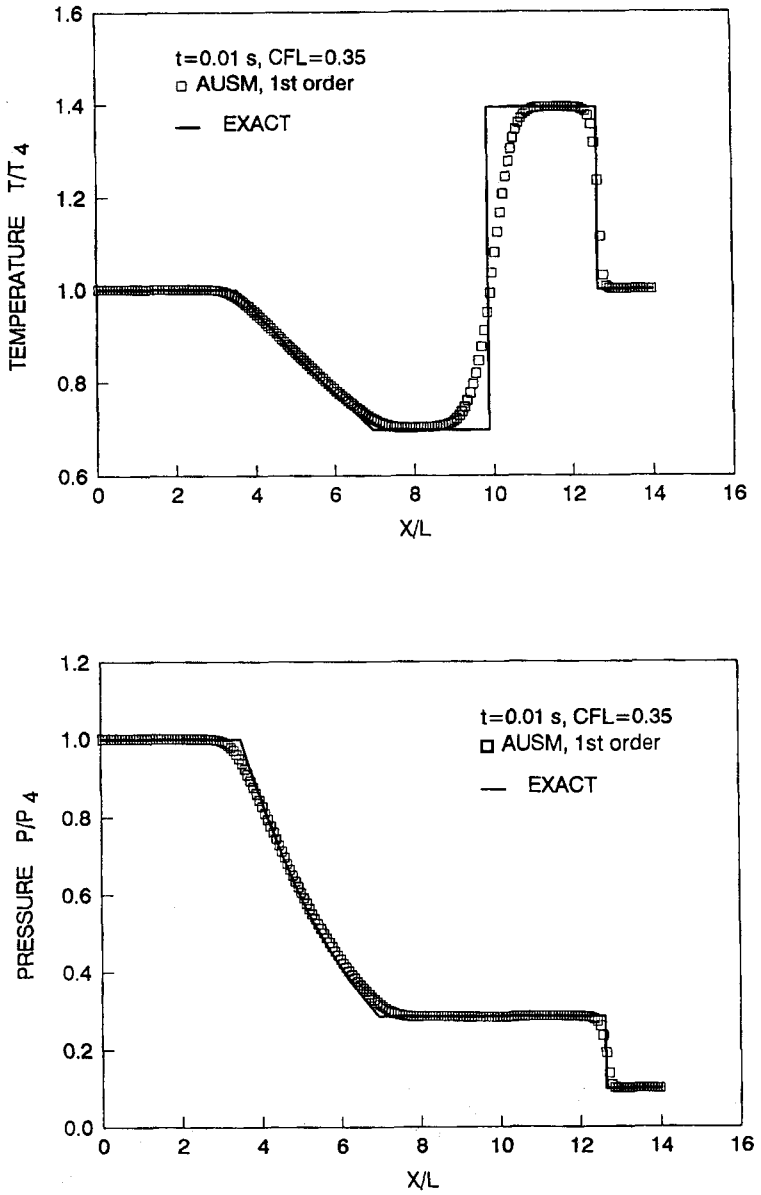

Figure 10. 1D shock tube results calculated by using AUSM scheme, grid size: 201, temperature and pressure

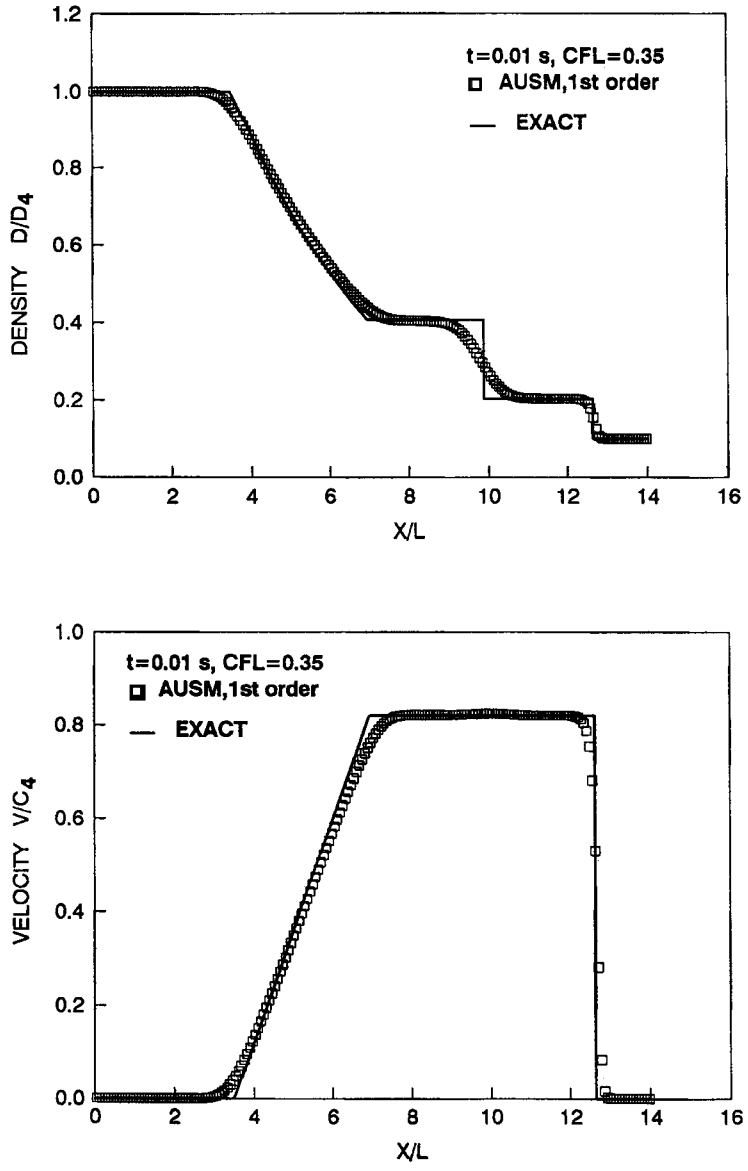

Figure 11. 1D shock tube results calculated by using AUSM scheme, grid size: 201, density and velocity

Figure 12. 2D grid of the inlet-diffuser, 101 × 31

are monotone without oscillations, overshoots or undershoots. But as mentioned before, because the pressure splitting is not continuously differentiable at the sonic point for the present and the AUSM scheme, a glitch appears at the sonic point position as Figure 13 shows. In contrast, the Van Leer scheme obtains the smooth transition at the sonic point. Fortunately, this drawback can be removed automatically by using higher-order differencing as it will be seen later. Figure 14 presents the pressure contours of the flow field. The present and the AUSM scheme gives the

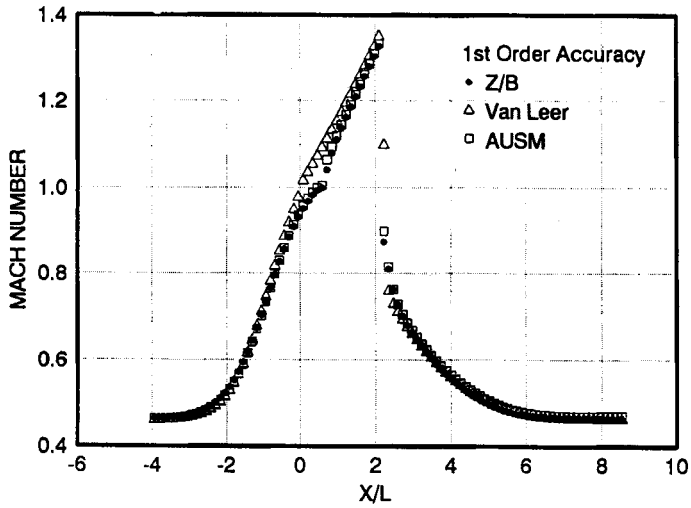

Mach Number Distributions along the Top Wall of the Inlet-Diffuser, Grid 101x31.

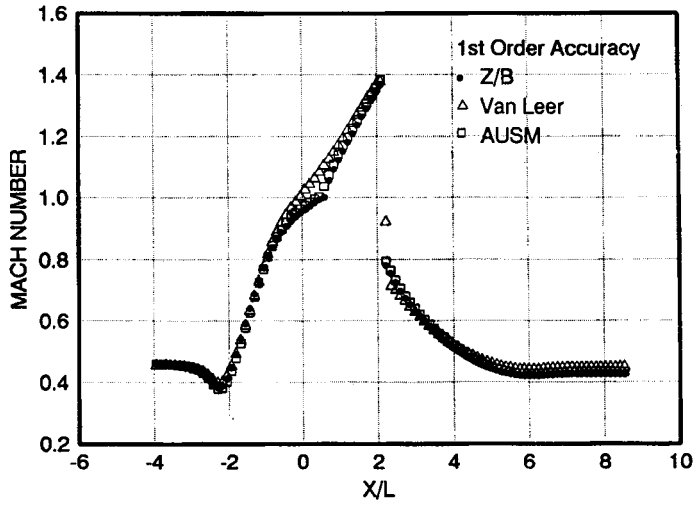

Figure 13. Mach number distributions along the walls of the inlet-diffuser with grid 101 × 31

sharper normal shock than the Van Leer scheme. The glitch at the sonic point was not revealed in the report of Liou and Steffen[11], who used the AUSM scheme with second-order differencing, except one case with first-order differencing, which was quasi-2D. The latter was not suitable to show the glitch.

In the next step, to see the performance of the present scheme for higher-order differencing, calculations were carried out using second-order differencing. MUSCL-type flux differencing[6] is used to evaluate the flux passing through the interface of a cell for the higher-order differencing. Again the explicit two-stage method was used for both the present and the AUSM scheme. Figure 15 shows the Mach number distributions using the fully upwind second-order scheme. It is seen that both the present and the AUSM scheme obtains the smooth transition at the sonic point and the glitch disappears. Furthermore, the shock profiles remain monotone without using any smooth limiters. The shock transition is almost in one zone at the top but it is two transition zones at the bottom. Figure 16 shows the pressure contours of the flow fields obtained by using the two schemes. It is seen that two pressure fields are almost indistinguishable and the shocks are sharp at the top and also at the bottom but with two zones.

To see the results with still higher-order differencing, computations were carried out with third-order biased upwind schemes. These results are obtained from the 3D solver using the URS[16,17] algorithm with the non-uniform grid in the 3D inlet-diffuser as shown in Figure 17. The computations were carried out in 3D, however the results are presented only for the central plane since the section is rectangular in spanwise direction and the results are nearly the same. In

Van Leer Scheme

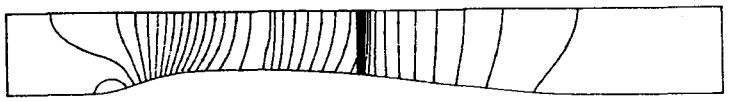

AUSM Scheme

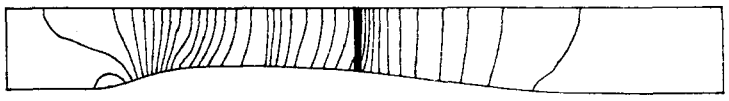

The Present Scheme

Figure 14. The pressure contours of the inlet-diffuser calculated by using the first-order differencing with grid 101×31

Figure 17, the bottom of the diffuser is shown at the top so that the geometry can be seen better. The lower figure shows the typical section in streamwise direction. The Mach number distributions along the top and bottom walls are presented in Figure 18. It can be observed that with all three schemes, oscillations appear in the vicinity of shock as expected.[6] The oscillation amplitude of present scheme (Z/B) is the smallest among the three schemes and those of the AUSM and Van Leer are almost the same. The smaller oscillation amplitude of the present scheme may be due to the fact that the present scheme is a Mach number polynomial of degree one, the lowest degree.

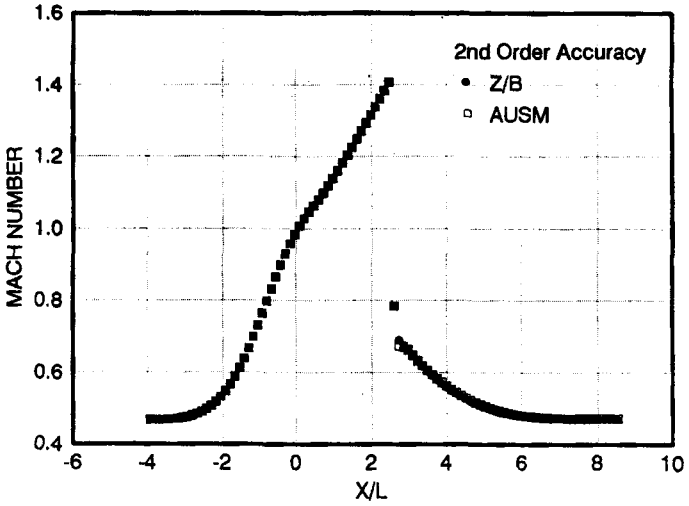

Mach Number Distrbutions along the Top Wall

of the Inlet-Diffuser, Grid 101x31.

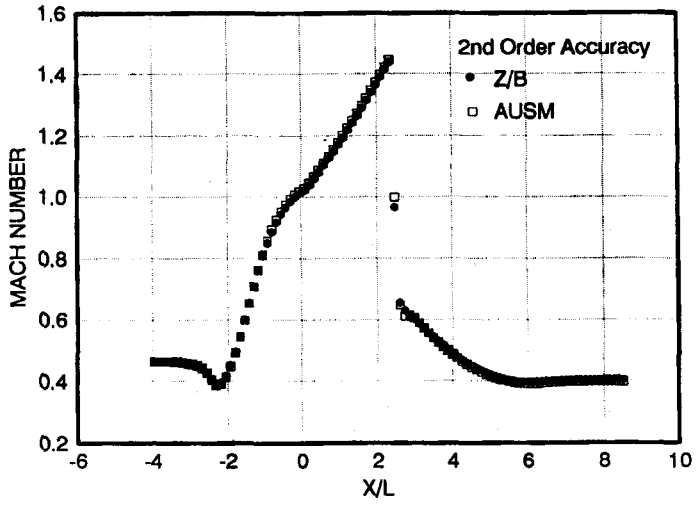

Figure 15. Mach number distributions along the walls of the inlet-diffuser with grid 101 × 31

The other two schemes are necessarily of degree two. The oscillations may be removed by using some smooth limiters to switch the scheme to lower differencing order at the shock location as many researchers have done in the past.[6,15] Such work is not done in the present paper. Once again, it can be seen in Figure 18 that a smooth transition at the sonic point is obtained by using third-order differencing and one transition zone shock profiles are obtained for all three schemes. In fact, the results of the present scheme completely agree with those from Van Leer and AUSM

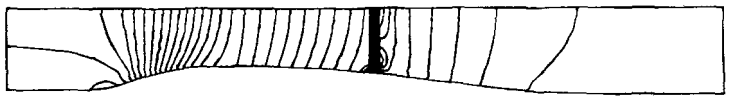

AUSM Scheme

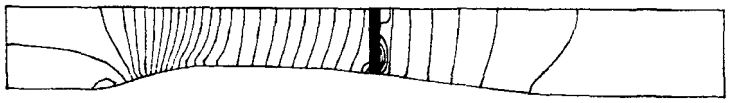

The Present Scheme

Figure 16. The pressure contours of the inlet-diffuser calculated by using the second order differencing with grid 101 × 31

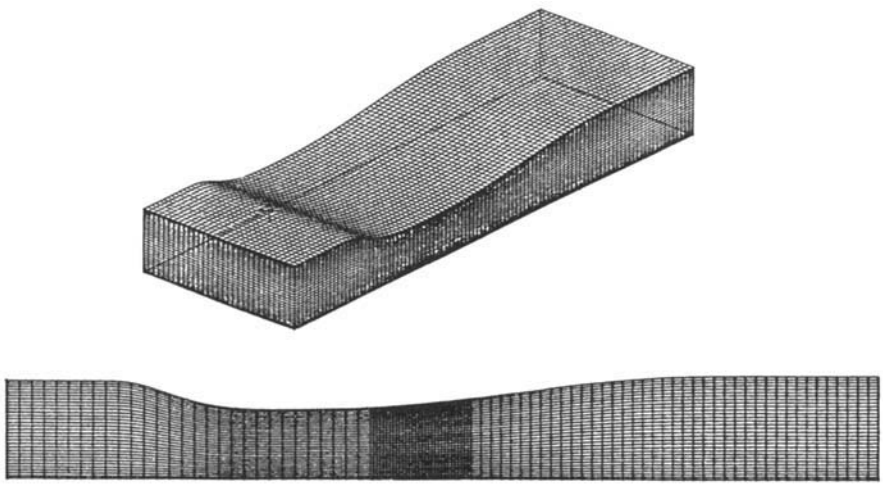

Figure 17. 3D grid of the inlet-diffuser with grid 101 × 31 × 31. To see the geometry, the bottom of the diffuser is shown at the top

except for the shock oscillations. The Mach number contours of the flow fields are presented in Figure 19. It is seen that all three look very similar with sharp shock waves. In comparison with Figures 14 and 16, some closed iso-Mach number lines appear at the top just before the shock waves, which are caused by the oscillations near the shock. It is also clear that the Van Leer scheme with third-order differencing produces sharper shock wave than the one with first-order differencing in Figure 14.

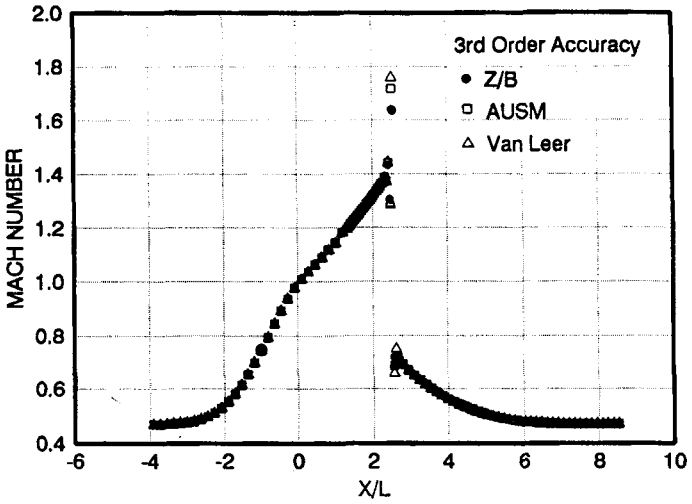

Mach Number Distribution along the Top Wall

of the Inlet-Diffuser, Grid 101x31.

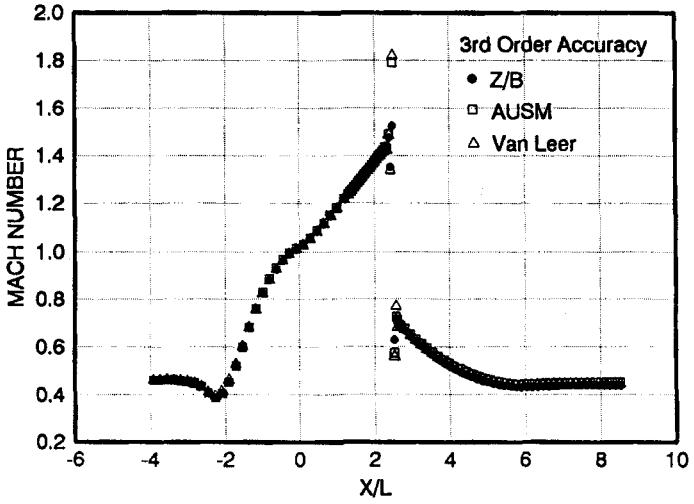

Figure 18. Mach number distributions along the walls of the inlet-diffuser with grid 101 × 31

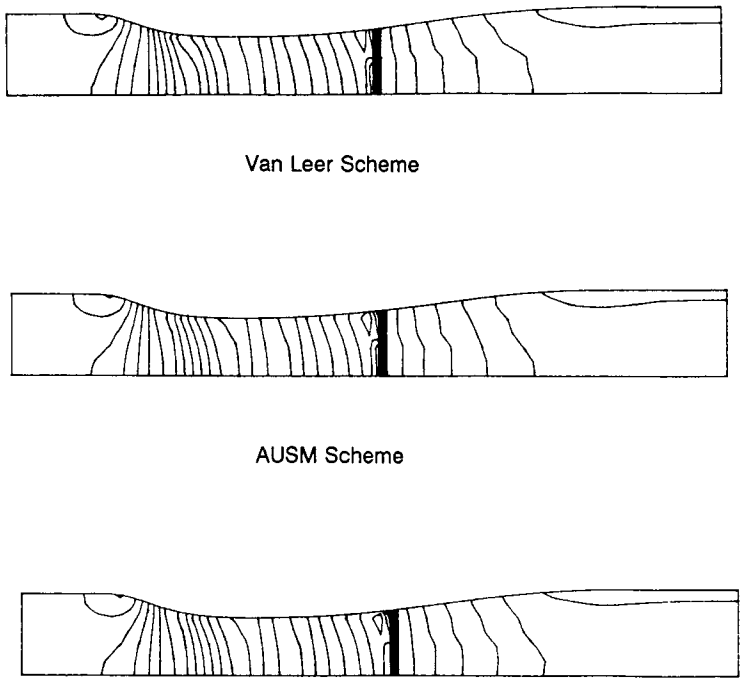

Figure 19. The Mach number contours of the inlet-diffuser calculated by using the third-order differencing with $101 \times 31 \times 31$

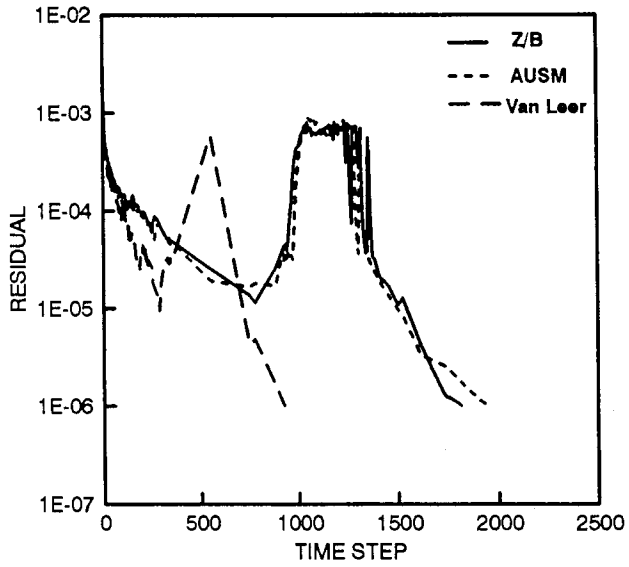

Figure 20. Convergence histories of the 3D inlet-diffuser by using the third order differencing

Figure 20 is the convergency histories for the 3D calculations of the inlet-diffuser. Single precision was used for the 3D calculations and the residuals were reduced to 10^{-6}. It is seen that the convergence rate of the Van Leer scheme is the best showing its advantage. Those of the present and AUSM schemes are almost the same, with time steps double that of the Van Leer

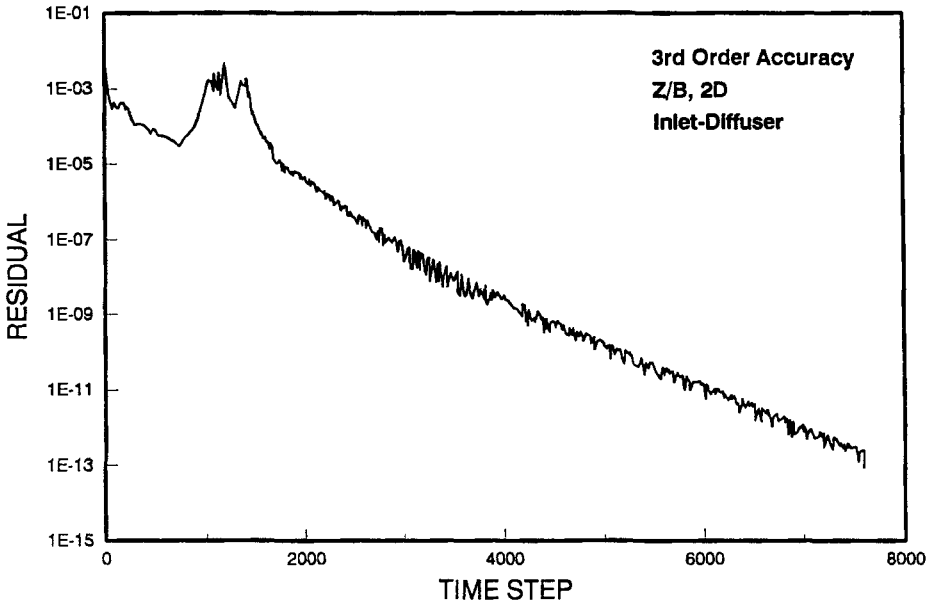

Figure 21. Convergence histories of the 2D inlet-diffuser by using the present scheme with grid 101 × 31

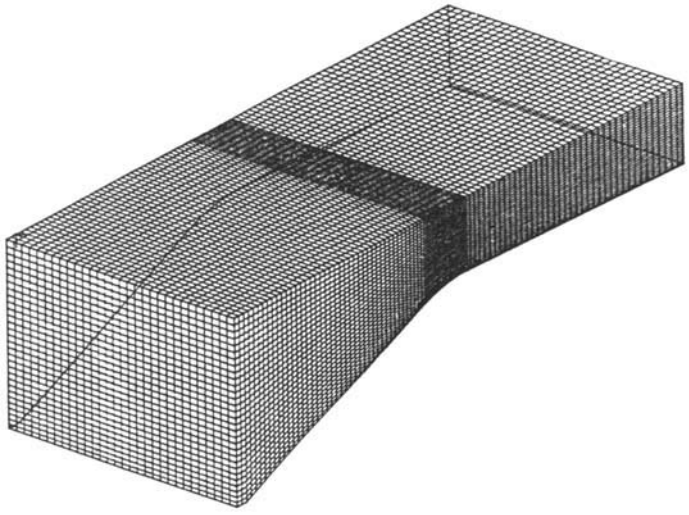

Figure 22. 3D grid of the transonic nozzle with grid 101 × 31 × 31. The grid shows the computational domain, which is the lower right side quarter of the nozzle

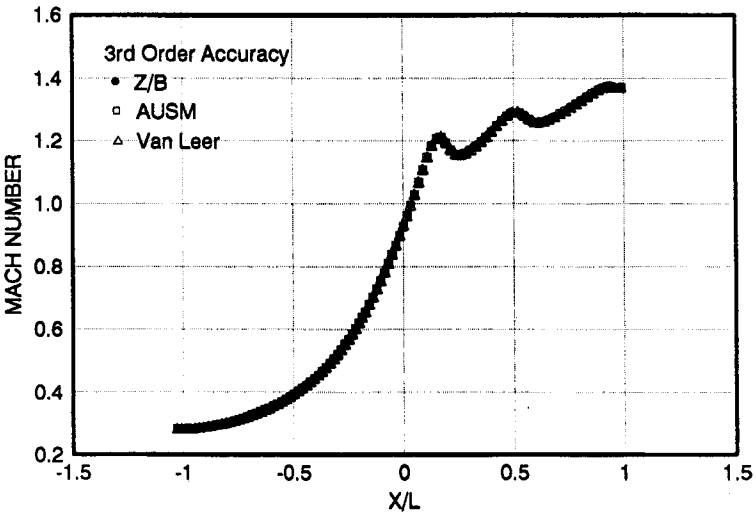

Figure 23. Mach number distributions along the bottom wall centreline of the transonic nozzle with grid $101 \times 31 \times 31$

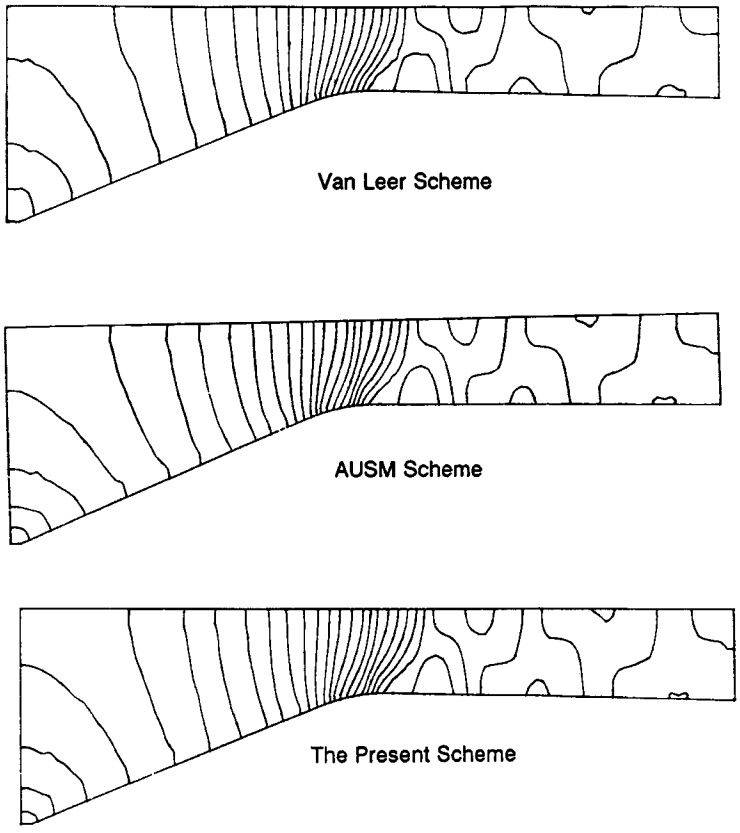

Figure 24. The Mach number contours of the transonic nozzle calculated by using the third order differencing with grid $101 \times 31 \times 31$

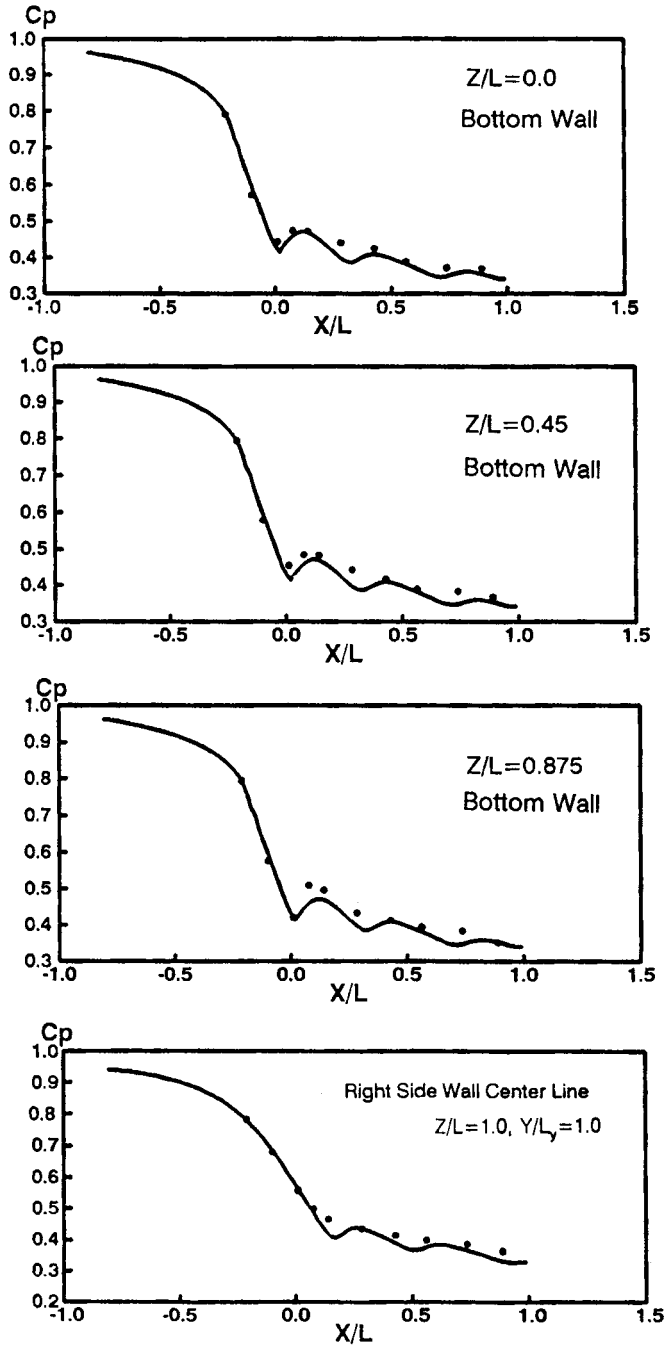

Figure 25. Pressure distributions of the transonic nozzle at four locations in spanwise directions

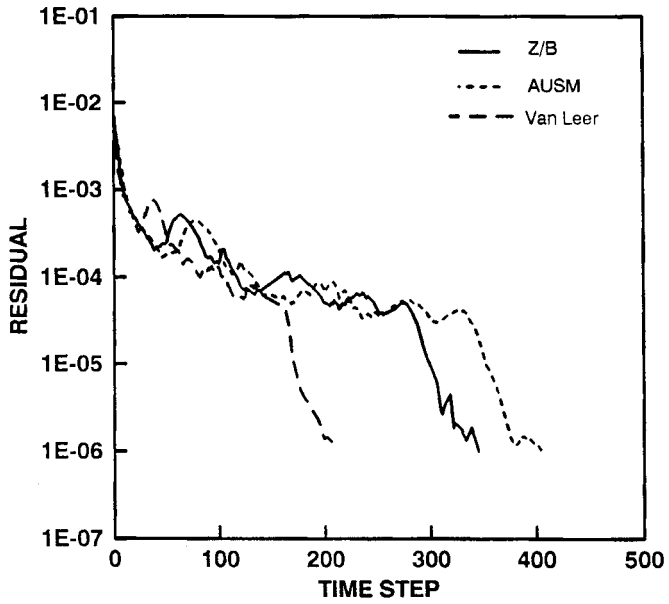

Figure 26. Convergence histories of the transonic nozzle with grid 101 × 31 × 31

scheme. For this case, the present scheme is a little faster than AUSM scheme. To see the convergence history with third-order accuracy in a 2D case, calculations were also carried out by using the upwind-relaxation algorithm for the 2D grid shown in Figure 12. Double precision was used and the residual was reduced to machine zero as shown in Figure 21. It is seen that after 10^{-5} accuracy, the residual decreases continuously, which shows that the present scheme converges without computational difficulties for this case.

Case 3: Case 3 is a study on a rectangular converging–diverging nozzle shown in Figure 22. Due to symmetry, it is sufficient to study the one quarter of the nozzle shown in the figure. Although this nozzle is 3D, it behaves almost like a 2D case for the variation in the spanwise direction is small. However, it is again a case solved by using 3D Euler equations and the results can be compared to experimental ones, in particular pressure distributions at various planes.[19] It is noted that there is no shock for this case. The computations were carried out by using the URS algorithm with third-order differencing for all three schemes and the results are compared. The Mach number distributions along the centre-line of the nozzle are presented in Figure 23 and the Mach number contours on the central plane in Figure 24. Figure 23 shows again that the present scheme completely agrees with Van Leer and AUSM scheme and the sonic transition is smooth. Figure 24 shows that the Mach contours are very similar with no discernible differences. Figure 25 is the pressure distributions of the nozzle at different spanwise locations. First three figures on the top are on the bottom wall of the nozzle and the last at the centreline as indicated in Figure 25. The results generally agree favourably with the experiment.[19] The pressure distributions at and near the central plane ($Z/L = 0{\cdot}0$ and $0{\cdot}45$) agree with the experiment better than that at $Z/L = 0{\cdot}875$. It may be because the real flow near the central plane mainly behaves as 2D flow. When it is near the side wall ($Z/L = 0{\cdot}875$), the interactions of the side wall boundary layers cause a strong 3D effect, which cannot be captured by using the 3D Euler equations. The disagreement is mainly at the throat where the flow has the tendency to separate. Similar results are seen on the

last figure in Figure 25, which illustrates the pressure distribution along the side wall centre-line. Figure 26 shows the convergency histories of the transonic nozzle with the grid of $101 \times 31 \times 31$. It is seen that for this case the present scheme is about 15% faster than AUSM and 70% slower than Van Leer scheme.

CONCLUDING REMARKS

A new flux vector splitting scheme has been suggested in this paper. This scheme uses the velocity component normal to the volume interface as the characteristic speed and yields the vanishing individual mass flux at the stagnation. The numerical dissipation for the mass and momentum equations vanishes with the mass flux. One of the diffusive term of the energy equation does not vanish at the stagnation. But the low numerical diffusion for viscous flows may be ensured by using higher-order differencing. Consequently, for the viscous flows, the present scheme may be more accurate than the flux vector splitting schemes without the mass flux vanishing at the stagnation. The scheme with the Mach number polynomial of degree one, the natural and lowest degree, is very simple and easy to be implemented.

The scheme has been tested to solve 1D, 2D and 3D Euler equations. The solutions are monotone and the normal shock wave profiles are crisp. For a 1D shock tube problem with the shock and the contact discontinuities, the present scheme and Roe scheme using the first-order differencing gave the most satisfactory results compared with those from Van Leer and Liou–Steffen's AUSM schemes. For the multidimensional transonic flows, the sharp monotone normal shock wave profiles with mostly one transition zone are obtained. A glitch appears at the sonic point when the first-order differencing is used for the transonic inlet-diffuser. But the glitch can be automatically removed by using a higher-order differencing. The scheme converges well for the tested cases, slightly faster than AUSM scheme and slower than Van Leer scheme. Generally, for the tested transonic flows, the results agree completely with the AUSM scheme and Van Leer scheme. However, using a third-order differencing, the present scheme produces results with least oscillations near the shock. The results also agree favourably with the experiment for a transonic nozzle.

ACKNOWLEDGEMENT

Mr. Fanming Meng has carried out some of the computations and prepared some figures, for which we would like to thank him.

REFERENCES

1. J. L. Steger and R. F. Warming, 'Flux vector splitting of the inviscid gasdynamics equations with application to finite-difference methods', *J. Comput. Phys.*, **40**, 263–293 (1981).
2. J. L. Thomas, B. Van Leer and R. W. Walters, 'Implicit flux-split schemes for the Euler equations', *AIAA J.*, **28**, 973–974 (1990).
3. J. L. Thomas and R. W. Walters, 'Upwind relaxation algorithms for the Navier–Stokes equations', *AIAA J.*, **25**, (1987).
4. G. C. Zha, D. Z. Liu and T. U. Ma, 'An efficient upwind/relaxation algorithm for the Euler and Navier–Stokes equations', *Int. j. numer. methods fluids*, **9**, 517–529 (1989) .
5. R. W. MacCormack, 'Current status of numerical solutions of the Navier–Stokes equations, *AIAA Paper 85-0032*, 1985.
6. W. K. Anderson, J. L. Thomas and B. Van Leer 'Comparison of finite volume flux vector splittings for the Euler equations', *AIAA J.*, **24**, 1453–1460 (1986).
7. B. Van Leer, J. L. Thomas, P. L. Roe and R. W. Newsome, 'A comparison of numerical flux formulas for the Euler and Navier–Stokes Equations', *AIAA Paper 87-1104*, 1987.
8. M. S. Liou and C. Steffen Jr, 'High order polynomial expansions for flux vector splitting', *Proc. Int. Conf. Computational Engineering Science*, 1991.

9. W. J. Coirier and B. Van Leer, 'Numerical flux formulas for the Euler and Navier–Stokes equations: II. Progress in flux-vector splitting', *AIAA Paper 91-1566-CP*, 1991.
10. D. Hänel and R. Schwane, 'An implicit flux-vector splitting scheme for the computation of viscous hypersonic flow', *AIAA Paper 89-0274*, 1989.
11. M.-S. Liou and C. J. Steffen, 'A new flux splitting scheme', *NASA TM 104404*, May 1991.
12. A. Harten, P. D. Lax and B. Van Leer, 'On upstream differencing and Godunov-type schemes for hyperbolic conservation laws', *SIAM Rev.*, **25**, 35–61 (1983).
13. G. C. Zha and D. Z. Liu, 'An efficient upwind relaxation-sweeping algorithm for three-dimensional Euler equations', *AIAA Paper 90-0129*, 1990.
14. G. C. Zha and E. Bilgen, 'An efficient upwind relaxation-sweeping algorithm for three dimensional Navier–Stokes equations', *AIAA Paper 92-0023*, 1992.
15. M.-S. Liou and A. T. Hsu, 'A time accurate finite volume high resolution scheme for 3D Navier–Stokes equations', *AIAA Paper 89-1994*, 1989.
16. E. A. John James, '*Gas Dynamics*', Allyn and Bacon, Newton, MA, 1984.
17. K. A. Hoffmann, '*Computational Fluid Dynamics for Engineers*', Engineering Education System™, 1989.
18. T. J. Bogar, M. Sajben and J. C. Kroutil, 'Characteristic frequency and length scales in transonic diffuser flow oscillations', *AIAA Paper 81-1291*, 1981.
19. M. L. Mason, L. E. Putnam and R. J. Re, 'The effect of throat contouring on two-dimensional converging–diverging nozzles at static conditions', *NASA TP-1704*, 1980.